

Article

## The Role of Aerosol-Cloud-Radiation Interactions in Regional Air Quality—A NU-WRF Study over the United States

Zhining Tao <sup>1,2,\*</sup>, Hongbin Yu <sup>2,3</sup> and Mian Chin <sup>2</sup>

<sup>1</sup> Universities Space Research Association, 7178 Columbia Gateway Dr., Columbia, MD 21044, USA

<sup>2</sup> NASA Goddard Space Flight Center, Greenbelt, MD 20771, USA;

E-Mails: hongbin.yu-1@nasa.gov (H.Y.); mian.chin@nasa.gov (M.C.)

<sup>3</sup> Earth System Science Interdisciplinary Center, University of Maryland, College Park, MD 20740, USA

\* Author to whom correspondence should be addressed; E-Mail: zhining.tao@nasa.gov.

Academic Editor: Evgueni Kassianov

Received: 31 March 2015 / Accepted: 24 July 2015 / Published: 30 July 2015

---

**Abstract:** This work assessed the impact of aerosol-cloud-radiation (ACR) interactions on U.S. regional ozone and PM<sub>2.5</sub> using the NASA Unified Weather Research and Forecasting modeling system. A series of three-month simulations have been carried out for the year 2010, in which the factor separation method has been applied in order to isolate the contributions from aerosol-radiation (AR), aerosol-cloud (AC), and their synergistic effects. The overall ACR effects were to reduce the average cloud liquid water path by  $25 \text{ g}\cdot\text{m}^{-2}$  (*ca.* 40% of the baseline) and to increase the downward shortwave radiation by  $8 \text{ W}\cdot\text{m}^{-2}$  (*ca.* 3% of the baseline). The spatial difference in response to ACR was large, with *ca.*  $50 \text{ W}\cdot\text{m}^{-2}$ , 1 K, and 100 m increases in downward shortwave radiation, surface temperature, and planetary boundary layer height (PBLH), respectively, while *ca.*  $60 \text{ g}\cdot\text{m}^{-2}$  decrease in cloud liquid water path in central Texas. The AC effect dominated for changes in downward shortwave radiation, cloud liquid water path, wind, and temperature, while both AC and AR effects contributed profoundly to PBLH change. As a result, surface ozone and PM<sub>2.5</sub> changed with large temporal-spatial variations. More than a 10 ppbv of surface ozone and a  $5 \mu\text{g}\cdot\text{m}^{-3}$  of PM<sub>2.5</sub> difference induced by ACR occurred frequently in the eastern U.S.

**Keywords:** aerosol-cloud-radiation interactions; air quality; factor separation; NU-WRF

---

## 1. Introduction

Aerosol, also known as particulate matter (PM), is an air pollutant that can adversely affect human health and impair visibility. Aerosol can also affect air quality through changing weather conditions that determine the level of surface concentration of PM and ozone. Aerosol absorbs and scatters radiation to perturb the atmospheric energy balance [1]. Absorbing aerosol heats the local atmosphere and cools the surface simultaneously, leading to a change in atmospheric stability and cloud formation [2]. Aerosol also serves as cloud condensation nuclei (CCN) and ice nuclei (IN) to modify cloud properties and precipitation processes [3]. Altogether, aerosol can affect the planetary boundary layer (PBL) structure [4–6] and the local/regional weather pattern [7–9], which can subsequently impact air quality.

Before the fully coupled online air quality model became available, air quality simulation had generally been carried out by an offline model that was driven by the meteorological parameters sampled at a fixed time interval from an independently run meteorology model [10]. Such offline simulations neglect feedback between atmospheric physics and chemistry such as the aerosol effects on cloud, radiation, and PBL structure. The advent of the fully coupled air quality models, such as the Multiscale Climate Chemistry Model [11], the Weather Research & Forecasting Model with Chemistry (WRF/Chem) [12], the Consortium for Small-scale Modeling with Aerosols and Reactive Trace gases (COSMO-ART) [13], and the models summarized by Baklanov *et al.* [14] and Jacobson [15], pave the way to examine the feedback among various atmospheric physical and chemical processes. For example, Zhang *et al.* [16] apply WRF/Chem to investigate the chemistry-aerosol-cloud-radiation-climate interactions over the continental United States (U.S.) and find that aerosols profoundly affect the local/regional surface temperature, PBL height (PBLH), wind, CCN, precipitation rate, and NO<sub>2</sub> photolysis rates. They urge the inclusion of accurate representations of such feedback in atmospheric models to reduce uncertainties in climate change prediction. Forkel *et al.* [17] also employ WRF/Chem to further their study of aerosol effects on regional air quality by separating out direct and indirect effects over Europe. They find that the aerosol-induced cloud cover change causes up to 4 ppb surface ozone change. While the direct aerosol effect tends to reduce the concentration of surface particulate matter with diameters of 10 µm or less (PM<sub>10</sub>) due to the increased PBLH, the indirect aerosol effect counteracts it by increasing surface PM<sub>10</sub> over a large part of continental Europe.

Despite the progress, the aerosol-cloud-radiation (ACR) interactions remain very uncertain [18] and the impact of aerosol on atmospheric composition and air quality is still in its infancy. The principle purpose of this work was to assess the impact of ACR interactions on U.S. regional air quality, focusing on ozone and PM with diameters less than 2.5 µm (PM<sub>2.5</sub>) in the late spring to early summer of 2010, using the NASA Unified WRF (NU-WRF) modeling system. The factor separation [19] method was applied in order to isolate the contribution from each individual interaction and that from the synergy between different interactions.

## 2. NU-WRF Modeling System, Set-up, and Experiment Design

NU-WRF is an observation-driven regional modeling system that has been developed from the advanced research versions of WRF [20] and WRF-Chem [12] with the addition of several NASA-developed components [21–23]. NU-WRF uniquely embeds the Land Information System as one land surface model option. The Goddard radiation and microphysics schemes in NU-WRF are the updated versions as compared to the ones in the community versions of WRF and WRF-Chem. The aerosol mass concentration calculated with the Goddard Chemistry Aerosol Radiation and Transport (GOCART) aerosol scheme [24] embedded in NU-WRF is used to calculate the CCN number concentration based on temperature/super-saturation [25,26] and the IN number concentration based on an empirical function of cloud temperature and aerosol concentration [27]. The estimated CCN and IN are only applied to the grid-scale cloud through the Goddard microphysics scheme, in which CCN affects the cloud-to-rain auto-conversion rate and IN influences the ice crystal-to-snow conversion rate and the growth of cloud liquid water to cloud ice. Without the ACR coupling, however, the Goddard microphysics scheme estimates cloud formation based on air temperature and water saturation, and calculates IN as a function of ice super-saturation. The cloud-to-rain auto-conversion is then calculated as a function of water content using a threshold approach, and the IN is used for calculation of the cloud ice mass. Aerosol mass concentrations for black carbon, organic carbon, sulfate, sea-salt, and dust are employed to calculate aerosol optical depth (AOD), single-scattering albedo, and asymmetry factor, which serve as inputs to a radiative transfer model to simulate aerosol interactions with radiation [28].

The experiment domain centered over the contiguous U.S. with a horizontal spatial resolution of 27 km. The simulation period was from 21 March to 30 June, 2010 and the analysis was based on the three-month (1 April–30 June) results, allowing the first ten days for the model spin-up. The key NU-WRF simulation set-up included the Goddard cloud microphysics [29] and the Goddard long/shortwave radiation scheme [30], the Noah land surface model [31], the Monin-Obukhov surface layer scheme, the Yonsei University planetary boundary layer scheme (YSU) [32], the new Grell cumulus scheme (an improved version of the ensemble cumulus scheme of [33]) that allows subsidence spreading for a high resolution simulation [34], and the second generation regional acid deposition model [35,36] for gas phase chemical mechanism. The lateral boundary conditions of meteorology were derived from the 6-h Final Operational Global Analysis data by the National Centers for Environmental Prediction. The chemical lateral boundary conditions were obtained from the Model for OZone and Related chemical Tracers (MOZART) [37] simulation updated every 6 h.

Anthropogenic emissions in this study were from the 2005 National Emissions Inventory (<http://www.epa.gov/ttnchie1/net/2005inventory.html>) compiled by the U.S. Environmental Protection Agency. Fire emissions were from the Fire Inventory from the National Center for Atmospheric Research version 1 (FINNV1) [38]. Biogenic emissions were calculated online using the Model of Emissions of Gases and Aerosols from Nature version 2 (MEGAN2) [39]. Dust emissions were estimated online based on surface wind speed, soil moisture, and the soil erodibility map [40]. Sea salt emissions were calculated online based on the parameterization by Gong [41].

The role of aerosol effects on meteorology and air quality is by nature nonlinear, such that the sum of change due to the aerosol-radiation (AR) interaction and due to the aerosol-cloud (AC) interaction is not necessarily equal to the overall change due to ACR interactions. The interactions among different factors may contribute an important portion to the overall aerosol effect. Therefore, in a nonlinear system, the total impact of one factor in the presence of other factors can be decomposed into the contribution from that factor alone (pure impact) and that from the synergy between that factor and others (synergistic impact). One good example of synergy is that the cloud change due to the AC interaction can lead to further changes in radiation that results from the AR interaction alone. To solve both pure and synergistic impacts of a factor, Stein and Alpert [19] develop the factor separation technique that has been successfully applied to various investigations [42–44]. In this study, we conducted four simulations (Table 1), each of which was a single continuous run for the entire simulation period. The impact of each individual factor and the synergistic effect can be derived as:

$$\text{Effect of aerosol-cloud interaction (denoted as AC)} = f_{AC} - f_0 \quad (1)$$

$$\text{Effect of aerosol-radiation interaction (denoted as AR)} = f_{AR} - f_0 \quad (2)$$

$$\text{Synergistic effect (denoted as SYN)} = f_{ACR} - f_{AC} - f_{AR} + f_0 \quad (3)$$

$$\text{Overall effect (denoted as ACR)} = f_{ACR} - f_0 \quad (4)$$

**Table 1.** Experiment design.

Experiment	Feedbacks Included	Simulation Results
NoACR	No aerosol-cloud-radiation interactions	$f_0$
AC	Aerosol-cloud interaction only	$f_{AC}$
AR	Aerosol-radiation interaction only	$f_{AR}$
ACR	Aerosol-cloud-radiation interactions	$f_{ACR}$

### 3. Results and Discussions

#### 3.1 Control Experiment (NoACR or $f_0$ ) and Model Evaluation

The meteorology responds profoundly to ACR interactions. In this study, we focused on several meteorological parameters that were most relevant to the surface air quality, including downward shortwave radiation, the temperature at 2 meters (T2), PBLH, cloud liquid water path (the vertical integration of cloud water content), and wind vector. These parameters directly impact the biogenic and dust emissions, photochemistry, horizontal/vertical transport, and mixing. Figure 1 shows the three-month average downward shortwave radiation, T2, PBLH, and cloud liquid water path from the NoACR experiment. Wind vectors at the surface, 850 mb, 700 mb, and 500 mb, were overlaid respectively on the downward shortwave radiation, T2, PBLH, and cloud liquid water path plots. As expected, the average T2 had a south-north gradient of about 20 K over the domain. The drier southwestern U.S. endured more than  $350 \text{ W}\cdot\text{m}^{-2}$  of downward shortwave radiation and less than  $1 \text{ g}\cdot\text{m}^{-2}$  of cloud liquid water path with the average PBLH well above 1000 m. The eastern U.S. generally experienced a shallower PBLH (a few hundred meters) and higher cloud liquid water path (more than  $35 \text{ g}\cdot\text{m}^{-2}$  over most areas). At the surface and lower atmosphere (e.g., 850 mb), the

northerly wind dominated over the Pacific coast. In the Gulf of Mexico, the prevailing wind blew from the east and veered north into Texas before turning east out to the Atlantic. In the free troposphere (e.g., 700 mb and 500 mb), the strong westerlies dominated the entire domain.

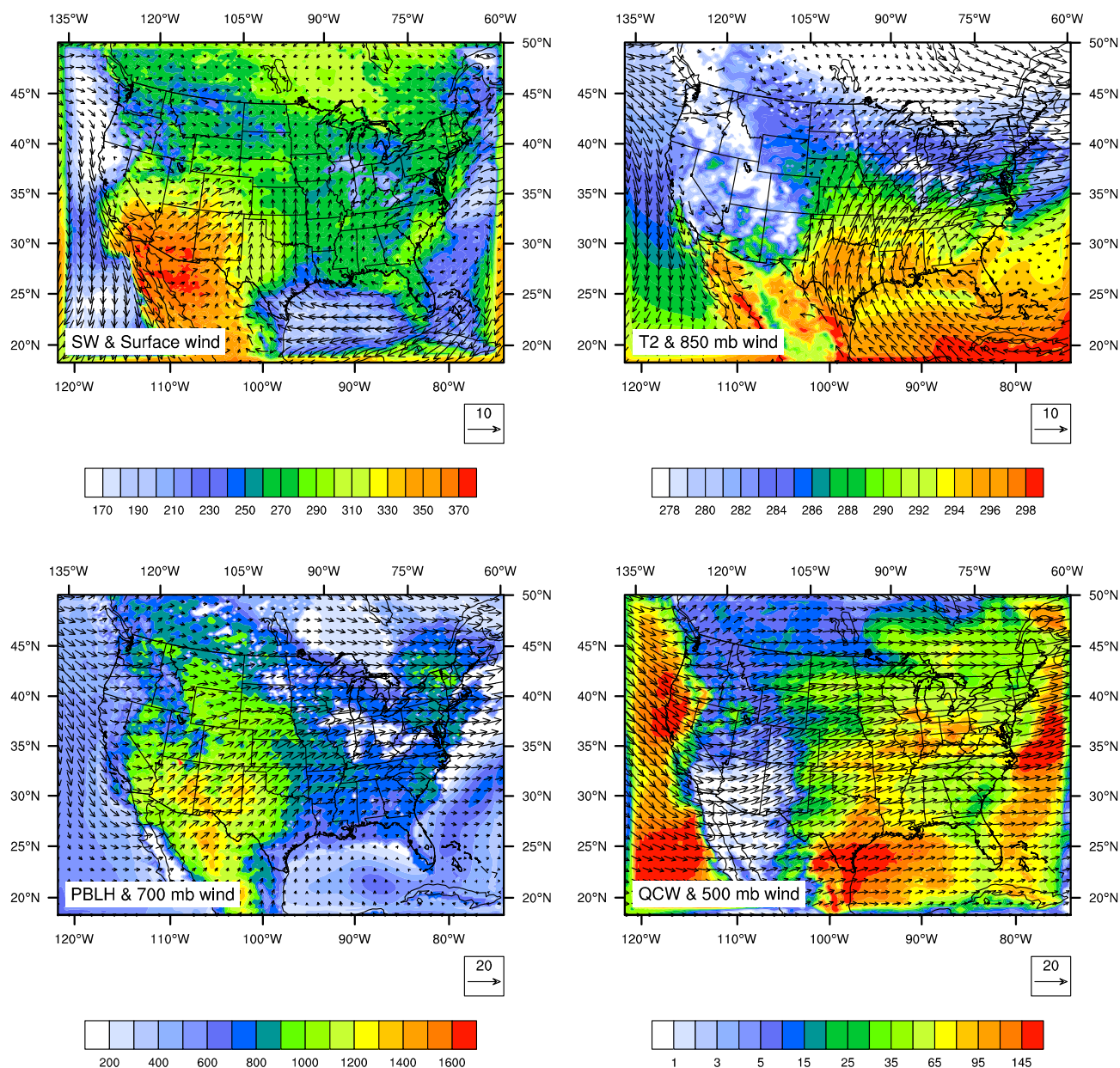


**Figure 1.** Spatial distributions of the three-month average downward shortwave radiation (SW,  $W \cdot m^{-2}$ ), T2 (K), planetary boundary layer height (PBLH, m), and cloud liquid water path (QCW,  $g \cdot m^{-2}$ ) from the experiment NoACR. The wind ( $m \cdot s^{-1}$ ) overlaying the above meteorological parameters is at surface 850 mb, 700 mb, and 500 mb, respectively.

Figure 2 illustrates the spatial distributions of the three-month average surface PM2.5, ozone, column AOD at 500 nm, and PM10 loading. Sea salt contributed mostly (>90%) to the high PM2.5 concentrations simulated over the Pacific near the U.S. west coast. It also accounted for more than 50% of PM2.5 over the Gulf of Mexico, the Atlantic, and the inland areas along the west coast. The high PM2.5 concentration (>20  $\mu g \cdot m^{-3}$ ) over the bordering areas of California and Arizona was almost

exclusively from the dust. The dust contribution, however, was mostly confined within the neighboring states of Nevada, New Mexico, and Utah. Over the vast eastern U.S. areas, the PM<sub>2.5</sub> was mainly composed of black/organic carbon and sulfate. AOD at 500 nm and PM<sub>10</sub> loading bore the similar spatial distribution as that of PM<sub>2.5</sub>, with the exception that AOD at 500 nm was low in the dust region where both high PM<sub>2.5</sub> and PM<sub>10</sub> loading were simulated. It was likely because of the low humidity over the dust areas. Since April through June was generally not the season with high ozone, moderate average ozone was simulated over the domain. The higher ozone (>45 ppbv) was modeled over the scatter areas in California, Arizona, Utah, Virginia, and North Carolina.

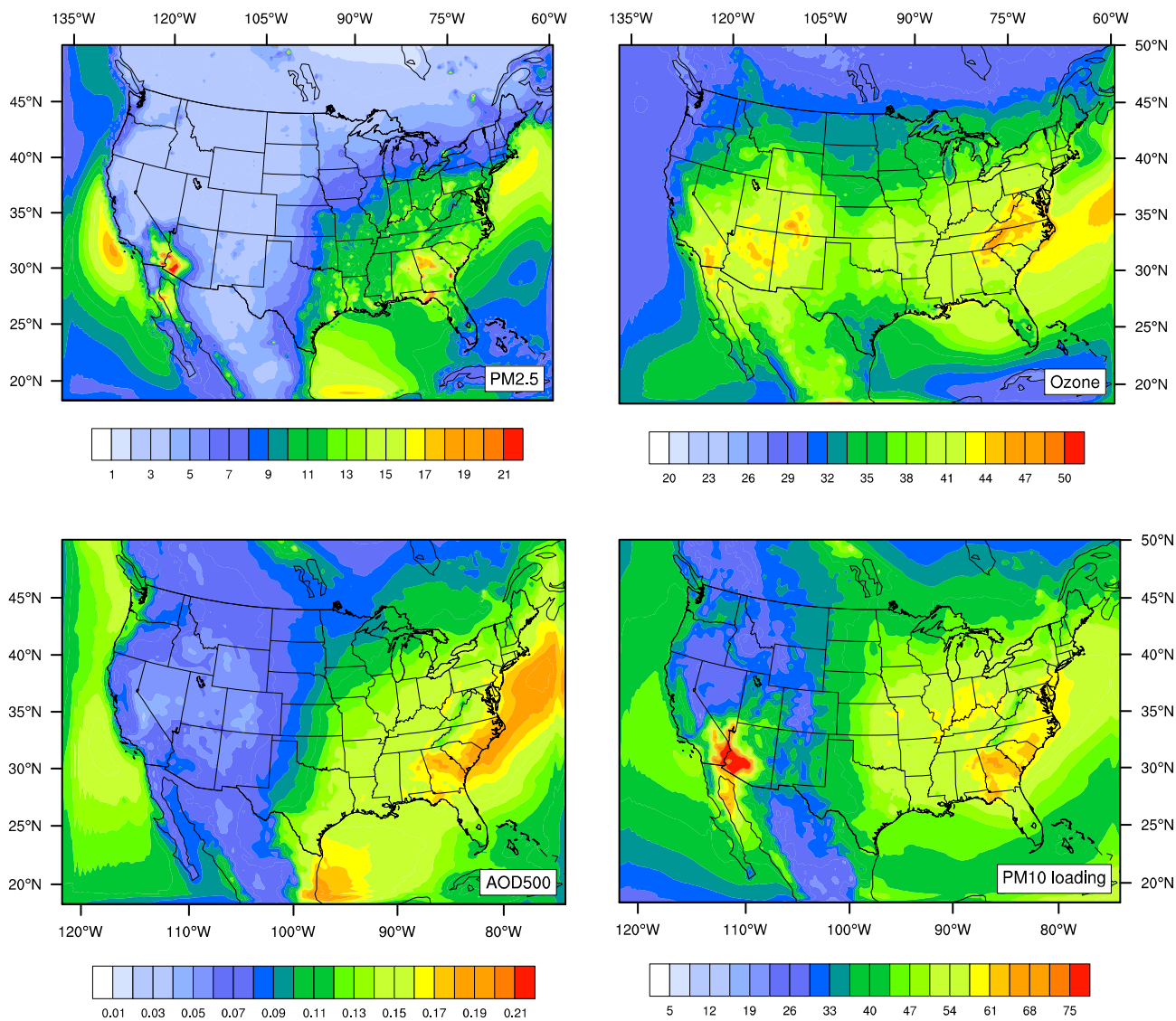


**Figure 2.** Spatial distributions of the three-month average surface PM<sub>2.5</sub> ( $\mu\text{g}\cdot\text{m}^{-3}$ ), ozone (ppbv), AOD at 500 nm, and PM<sub>10</sub> loading ( $\text{mg}\cdot\text{m}^{-2}$ ) from the experiment NoACR.

Previous studies have shown that NU-WRF has sufficient skills in simulating land-atmosphere exchange, aerosol-cloud-radiation interactions, atmospheric photochemical processes, and air quality [21–23,28]. In this study, we compared the daily precipitation from the control experiment to the rain gauge data analyzed by the Climate Prediction Center of the National Oceanic and Atmospheric Administration under its unified precipitation project [45,46]. Figure 3 shows the

geographic distribution of the observed and modeled three-month average precipitations. In general, NU-WRF captured the spatial pattern of the average precipitation over the continental U.S. with large rainfalls along the northwest Pacific coast and in the Midwest. However, NU-WRF appeared to overestimate the precipitation by up to a factor of three over the northwest Pacific coast, while underestimating it in the southeastern U.S. by up to a factor of two. The domain average precipitation from the rain gauge data was  $1.98 \text{ mm}\cdot\text{day}^{-1}$  averaged over three months as compared to a  $2.10 \text{ mm}\cdot\text{day}^{-1}$  obtained from the NU-WRF simulation. Out of the 750,386 observed precipitation incidents (grid-day), NU-WRF caught *ca.* 65% of them with the remaining 35% being either missed (*i.e.*, positive observed but zero modeled rainfalls, 8.5%) or false alarms (*i.e.*, zero observed but positive modeled rainfalls, 26.5%). The comparison of the precipitation out of the ACR experiment ( $f_{ACR}$ ) to the observation showed very similar statistics with approximately a 64% hit rate.

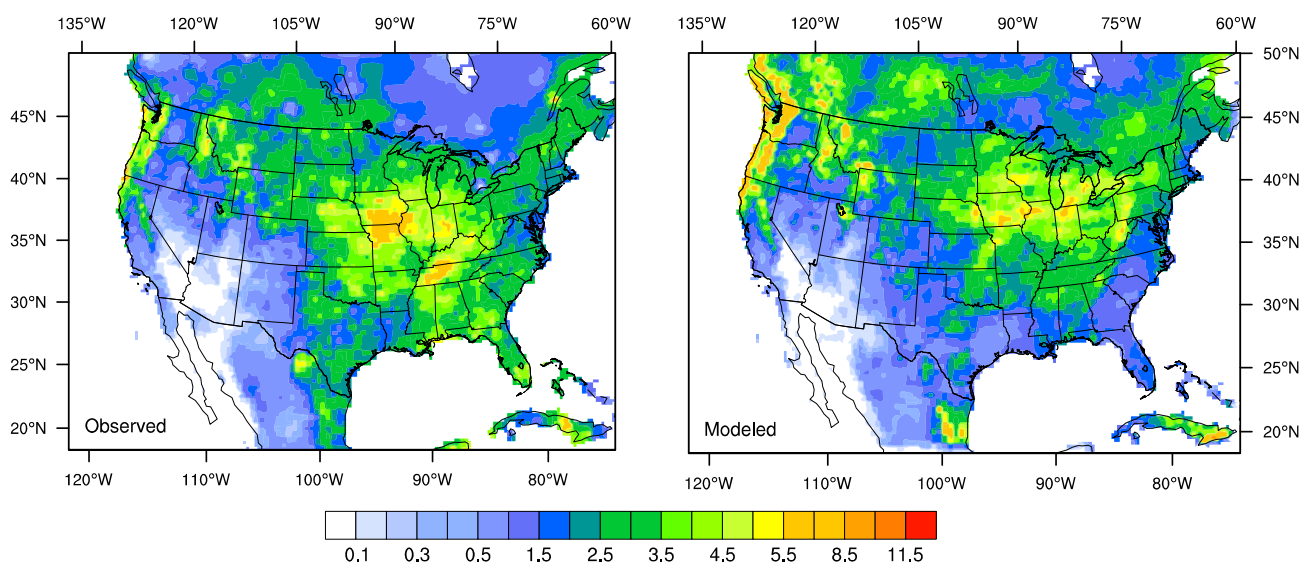


**Figure 3.** Spatial distribution of three-month average daily precipitations (mm) from the rain gauge measurements (**left**); and NU-WRF NoACR experiment (**right**).

**Table 2.** Comparison of NU-WRF simulated near surface ozone/PM2.5 concentrations and AOD at 500 nm to the respective observation \*.

Species	Number of Grid Cells	Normalized Bias (%)		Normalized Gross Error (%)	
		Range	Domain	Range	Domain
<b>Control (Exp. NoACR)</b>					
Ozone	883	-28.2~31.6	-3.3	11.8~31.6	18.2
PM2.5	458	-68.7~174.4	21.6	33.1~176.6	60.1
AOD	45	-65.6~20.8	-20.7	19.4~65.6	43.1
<b>Exp. ACR</b>					
Ozone	883	-28.2~28.0	-2.8	11.9~29.7	18.8
PM2.5	458	-68.3~176.6	23.4	35.0~178.8	61.3
AOD	45	-65.6~19.7	-19.6	19.3~65.6	43.1

\*  $Normalized\ Bias = \frac{1}{N} \sum_{i=1}^N \frac{M_i - O_i}{O_i} \times 100\%$  ;  $Normalized\ Gross\ Error = \frac{1}{N} \sum_{i=1}^N \left| \frac{M_i - O_i}{O_i} \right| \times 100\%$  , where  $N$  is the number of observations, and  $M$  and  $O$  are modeled and observed values, respectively.

We also compared the hourly surface PM<sub>2.5</sub> and ozone concentrations to the Air Quality System observations (<http://www.epa.gov/ttn/airs/airsaqs/>), as well as evaluated the daily AOD against the measurements from the Aerosol Robotic Network level 2 product that was cloud-screened and quality-assured (<http://aeronet.gsfc.nasa.gov/>) as shown in Table 2. Overall, NU-WRF simulated the surface ozone well with the domain-averaged normalized bias as  $-3.3\%$  and the average normalized gross error within 19%. Of the 883 model grids where ozone observation was available, more than 80% had less than 20% normalized gross error, and 74% had normalized bias within 10%. The NU-WRF performances on surface PM<sub>2.5</sub> and column AOD at 500 nm were less satisfactory, with the domain-averaged normalized bias around 22% and  $-21\%$  and normalized gross error 60% and 43%, respectively. The inclusion of the ACR interaction in the simulation, as expected, improved the performance at some locations but made no difference or even worse at some other locations. Overall, taking into account the ACR interactions marginally reduced the normalized bias for ozone and AOD at 500 nm but increased it for PM<sub>2.5</sub> (Table 2). The usage of 2005 emissions for the 2010 simulation would surely cause some errors and the uncertainty associated with the meteorology modeling may also contribute to the bias. The pinpoint of the exact reason is beyond the scope of this research. Nevertheless, this study focused on the difference between experiments and the relatively large normalized bias and normalized gross error for PM<sub>2.5</sub> and AOD were not anticipated to impair the major conclusion.

### 3.2. Impact on Meteorology

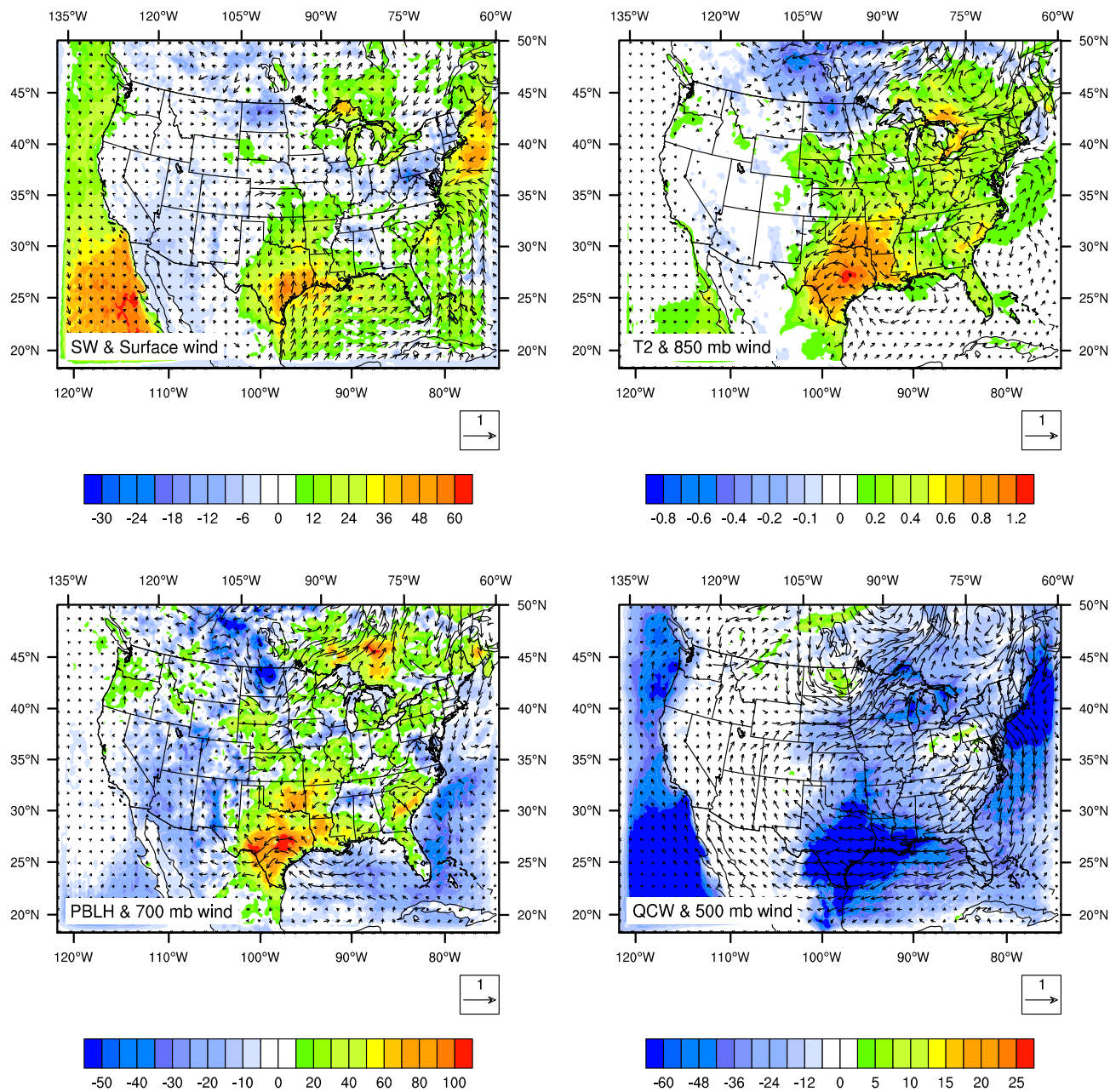
#### 3.2.1. Overall Effect of Aerosol-Cloud-Radiation Interactions (ACR)

Figure 4 illustrates the ACR effects on the meteorological variables averaged over three months. The ACR effect was to increase the three-month average downward shortwave radiation by 20–60  $\text{W}\cdot\text{m}^{-2}$  over the vast ocean areas. A large downward shortwave radiation increase was also seen over the eastern to central Texas, Oklahoma, Arkansas, Louisiana, the southern Mississippi, Florida, and to the north of the Great Lakes. A 0–30  $\text{W}\cdot\text{m}^{-2}$  reduction in downward shortwave radiation was simulated in other areas of the domain. The spatial distribution of downward shortwave radiation changes normally closely linked to that of cloud liquid water path changes—a decrease in cloud liquid water path, and thus the cloud coverage—resulted in an increase in downward shortwave radiation, and *vice versa*. In the scattered areas of the eastern U.S. (e.g., the southern Pennsylvania), the reduction in downward shortwave radiation appeared mainly due to increased PM loading (figure not shown).

The changes in atmospheric energy due to ACR would lead to changes in atmospheric temperature (represented by T2 for the analysis) and PBLH. T2 response to the ACR effect varied spatially: while a negligible average T2 (within 0.2 K) change was simulated over the ocean and the vast western U.S. areas, a 0.2 to more than 1 K increase was modeled over the eastern U.S., and up to a 0.8 K decrease was seen in the central northern portion of the domain. PBLH change closely related to the T2 change spatially with up to a 100 m increase in the central Texas and a 50 m decrease in the north Dakota.

The atmospheric circulation responded to the energy change as well. Near the surface (surface and 850 mb), the ACR effect generally strengthened the wind blowing from the Gulf of Mexico to Texas by *ca.*  $0.5\text{ m}\cdot\text{s}^{-1}$ , averaged over three months, and weakened the west wind in the northeast U.S. In the free troposphere, especially at 500 mb, the ACR effect normally enhanced the average westerly wind

in the central to northern portions of the domain, but weakened it by up to  $1 \text{ m}\cdot\text{s}^{-1}$  in the southern domain. The domain average changes in the downward shortwave radiation, cloud liquid water path, T2, PBLH, wind, and PM2.5 loading are listed in Table 3. The next few sections detail the analysis of the AR vs. AC effect on meteorology and provide more insight on how aerosols perturb the weather system and the resulting impacts on regional air quality.



**Figure 4.** Spatial distribution of changes in the three-month average downward shortwave radiation (SW,  $\text{W}\cdot\text{m}^{-2}$ ), T2 (K), planetary boundary layer height (PBLH, m), and cloud liquid water path (QCW,  $\text{g}\cdot\text{m}^{-2}$ ) due to ACR. The changes in wind ( $\text{m}\cdot\text{s}^{-1}$ ) overlaying the above meteorological parameters are at surface 850 mb, 700 mb, and 500 mb, respectively.

**Table 3.** Overall ACR effect and percentage contributions from individual factors of AC, AR, and SYN <sup>a</sup>.

	SW	QCW	T2	PBLH	Wind at 850 mb	Wind at 500 mb
ACR	8.16 ( $W \cdot m^{-2}$ )	-25.3 ( $g \cdot m^{-2}$ )	0.10 (K)	0.39 (m)	-0.054 ( $m \cdot s^{-1}$ )	-0.052 ( $m \cdot s^{-1}$ )
AC (%)	73.4	-95.6	69.2	51.2	-57.9	-57.7
AR (%)	-25.5	2.6	-26.9	-48.7	-17.3	-17.7
SYN (%)	1.1	-1.8	-3.9	0.1	24.8	24.6

<sup>a</sup> Only the ACR row shows the value (Exp. ACR–NoACR) with the corresponding unit. SW = downward shortwave radiation; QCW = cloud liquid water path.

### 3.2.2. Effect of Aerosol-Radiation Interaction (AR)

Aerosols not only directly absorb and/or scatter solar radiation but also change atmospheric heating rates and cloud formation and distribution, which would lead to further alteration of atmospheric energy balance. This so-called AR effect was investigated following the factor separation method. Overall, the AR effect was to reduce the downward shortwave radiation by 6~20  $W \cdot m^{-2}$  in most areas of the domain and to increase it by up to 20  $W \cdot m^{-2}$  in some places, especially to the north of the Great Lakes and in the North Atlantic ocean off the east coast of South Carolina to Massachusetts (Figure 5). The aerosol scattering and absorption of radiation represented by PM loading and AOD (Figure 2) can partially explain this change. In most land areas, the increased PM loading due to AR led to a reduction in downward shortwave radiation and *vice versa*. In Texas, the eastern Kentucky and Tennessee, and the mid-Atlantic Ocean (from Virginia to New York), however, the AR-induced cloud change may mainly contribute to the changes in the downward shortwave radiation. For example, the downward shortwave radiation decreased by up to 20  $W \cdot m^{-2}$ , nearly 10% of the three-month average based on the NoACR experiment, in the eastern Texas but the PM loading stayed relatively unchanged there. Therefore, the cloud change as represented by the cloud liquid water path change in Figure 5 was mainly responsible for the downward shortwave radiation reduction there. It was found that more cloud was formed in Texas that tended to reflect more solar radiation back to the space, while less cloud was present in the mid-Atlantic Ocean that allowed more solar radiation to reach the surface. In the regions where aerosol absorption and scattering contributed markedly to the downward shortwave radiation reductions, the aerosol-induced cloud effects generally enhanced the reduction. For example, in Pennsylvania, the greater presence of cloud due to AR interaction further decreased the downward shortwave radiation that had already been reduced by the aerosol itself. The relative contribution of the aforementioned aerosol effects, *i.e.*, aerosol itself *vs.* its induced cloud change, to the downward shortwave radiation change cannot be determined in this study, but Forkel *et al.* [17] point out that, in Europe, the downward shortwave radiation change due to AR is mostly linked to changes in cloud cover induced by aerosols. The domain-average changes in the downward shortwave radiation and cloud liquid water path were  $-4.2 W \cdot m^{-2}$  (reduction) and  $0.7 g \cdot m^{-2}$ , respectively.

Except for a few scattered locations, AR reduced T2 and PBLH (Figure 5). 0.1~0.4 K decreases in the three-month average T2 were seen across large portions of the domain, with up to 0.8 K reduction found in a location around 48N and 102W of Canada. PBLH generally decreased upon the reduced surface sensible heat flux and increased on the enhanced one (figure not shown). This was understandable because the buoyancy fueled by surface heating was the primary driving force for PBL

growth [22]. The domain-average changes of T2 and PBLH due to AR were  $-0.07$  K and  $-7.1$  m (reduction), respectively.

The AR effect tended to weaken the surface wind blowing from the Gulf of Mexico to Texas and to reduce the air movement out of the northeast U.S. into the Atlantic. This condition favored the pollution built-up in the aforementioned already polluted areas. In the free troposphere (700 mb and 500 mb), the AR effect was generally to weaken the western wind in the east U.S. It was worth noting that the wind change induced by the AR effect allowed more moist air from the oceans into the land in the free troposphere. The moist air typically converged in the regions covering Texas and Louisiana, as well as in the northeast to midwest U.S. This may contribute to the enhanced cloud liquid water path found in those areas.

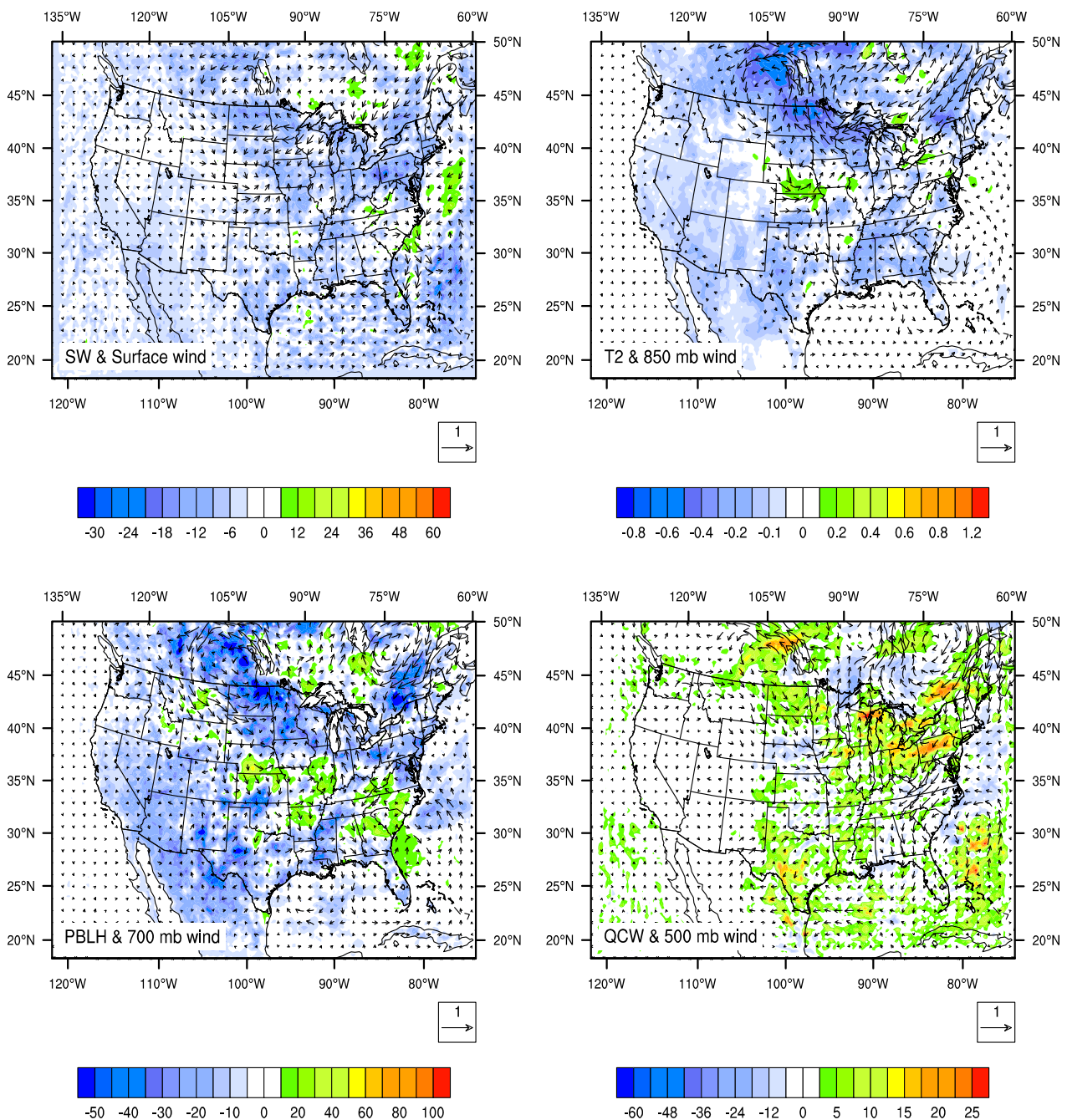


Figure 5. Same as Figure 4 except for changes due to AR.

### 3.2.3. Effect of Aerosol-Cloud Interaction (AC)

Compared with the AR effect, the AC effect was more pronounced, as illustrated in Figure 6. Over the ocean and central U.S. from Minnesota to Texas, approximately  $40\text{--}60\text{ g}\cdot\text{m}^{-2}$  less cloud liquid water path averaged over three months was simulated when turning on AC. Meanwhile, the rainwater content generally experienced a  $2\text{--}10\text{ g}\cdot\text{m}^{-2}$  increase with around  $2\text{ million}\cdot\text{mm}^{-2}$  increase of CCN. As a result, the three-month total precipitation increased by 10 to 100 mm in those regions. Tao and Li [47] summarize three possible mechanisms (latent heating, cool pool, and cold microphysics) that explain the CCN effect on precipitation. They point out that the enhanced latent heat release due to a higher CCN concentration can create stronger updrafts/downdrafts, which may lead to more precipitation. In addition, a higher CCN concentration can result in more but smaller clouds and raindrops, prompting a stronger evaporative cooling to enhance the strength of the near-surface cool pool. The convergence could become stronger when the enhanced cool pool interacts with low-level wind shear, which would produce a more vigorous convection and lead to more surface precipitation. Though the detailed analysis of how increased CCN impacts precipitation was beyond the scope of this study, the enhanced precipitation simulated in this study due to the higher CCN concentration was likely the result of the combined aforementioned effects. The reduced cloud liquid water path due to more precipitation induced by the AC effect allowed more downward shortwave radiation but less downward longwave radiation over the regions. It simulated up to  $60\text{ W}\cdot\text{m}^{-2}$  more of the three-month average downward shortwave radiation and  $8\text{ W}\cdot\text{m}^{-2}$  less average downward longwave radiation in the Pacific next to Baja California Peninsula. The changes in the downward shortwave radiation and cloud liquid water path averaged over the entire domain were  $12.2\text{ W}\cdot\text{m}^{-2}$  and  $-25.5\text{ g}\cdot\text{m}^{-2}$ , respectively, much larger than those induced by AR (Table 3). The finding of less cloud formation but higher rainwater content due to AC agreed with the finding by Forkel *et al.* [17], which was also supported by a study by Yang *et al.* [48] who simulated a lower cloud optical depth and cloud liquid water path for the south Pacific when considering AC.

The radiation change due to AC caused an increase of  $0.1\text{--}1.2\text{ K}$  in the three-month average T2 across most areas to the east of the Rocky Mountains, with the largest increase found in the eastern Texas. The average PBLH increased by 10 to more than 100 m over the land areas where T2 increased, but endured a moderate decrease (10–40 m) over the ocean. The domain-average changes of T2 and PBLH due to AC were  $0.18\text{ K}$  and  $7.5\text{ m}$  (increase), respectively, opposite to the changes induced by AR.

The wind field responded to the AC effect differently at different altitudes. In the near-surface (surface and 850 mb) atmosphere, the AC effect strengthened the south-southeast wind off the Gulf of Mexico into Texas and weakened the south wind from Texas to Oklahoma, while it reduced the airflow from the northeast U.S. out to the Atlantic. In the free troposphere (700 and 500 mb), the AC effect generally enhanced the west wind in the central U.S. but reduced it in the southern and northern U.S. on a relatively small scale (less than 5%).

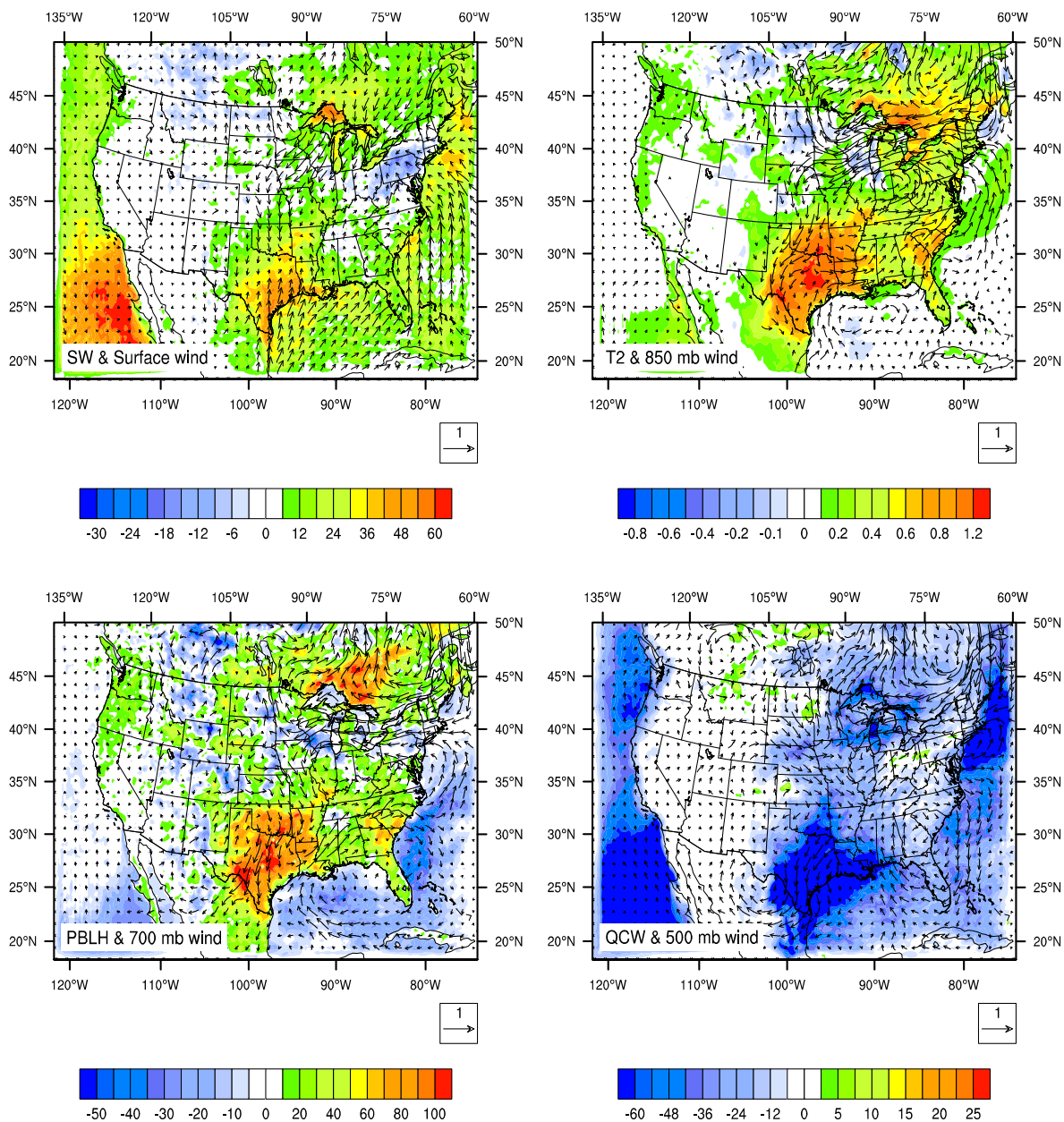
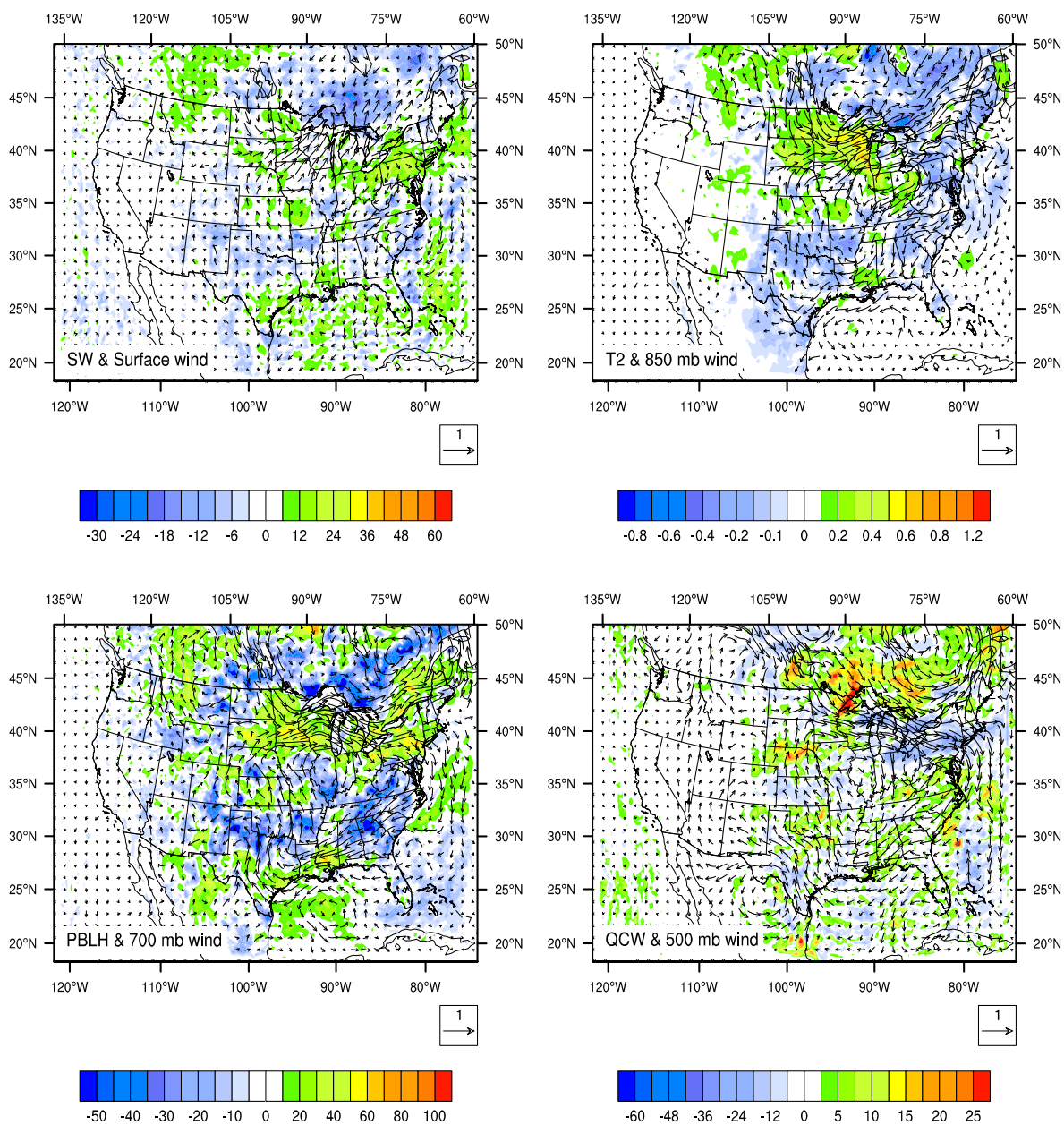


Figure 6. Same as Figure 4 except for changes due to AC.

### 3.2.4. Synergistic Effect between AR and AC (SYN)

Following the factor separation technique (Equation (3)), SYN was calculated, which can increase or decrease the impact of each individual factor and be potentially important in a nonlinear system. Figure 7 illustrates what happens when such a synergistic effect is taken into account. SYN caused the reductions in both PM10 loading (up to  $2 \text{ mg} \cdot \text{m}^{-2}$ ) and the cloud liquid water path (approximately  $20 \text{ g} \cdot \text{m}^{-2}$ ) over Pennsylvania and New York, which allowed *ca.*  $24 \text{ W} \cdot \text{m}^{-2}$  more downward shortwave radiation. These changes somewhat counteracted the impacts due to AC and AR in the aforementioned areas. In the eastern Texas, SYN enhanced the downward shortwave radiation by about  $10 \text{ W} \cdot \text{m}^{-2}$ , which amplified the downward shortwave radiation change due to AC but counteracted the change due to AR. On the domain average, SYN decreased the cloud liquid water path by  $0.49 \text{ g} \cdot \text{m}^{-2}$  but increased the downward shortwave radiation by  $0.19 \text{ W} \cdot \text{m}^{-2}$ . The domain-average T2 and PBLH stayed

relatively unchanged, with  $-0.01$  K and  $0.01$  m difference, respectively, although local ups and downs were still observed with a positive relation between T2 and PBLH, *i.e.*, increased/decreased T2 generally came with the increased/decreased PBLH.



**Figure 7.** Same as Figure 4 except for changes due to SYN.

### 3.2.5. Relative Contribution of AR, AC, and SYN

Table 3 also listed the percentage contributions from AC, AR, and SYN to ACR averaged over the entire domain based on Equation (5),

$$\% factor = \frac{factor}{|AC| + |AR| + |SYN|} \times 100\% \tag{5}$$

where *factor* can be AC, AR, or SYN. The same/opposite sign of an individual factor and ACR indicated that the *factor* contributed positively/negatively to the overall effect. The absolute value of

the percentage contribution suggested the relative importance of the *factor* in the overall effect. It was seen that the ACR effect on meteorology was to increase the domain-average downward shortwave radiation, T2, and PBLH by  $8.16 \text{ W}\cdot\text{m}^{-2}$ , 0.10 K, and 0.39 m, respectively, but to decrease the cloud liquid water path by  $25.3 \text{ g}\cdot\text{m}^{-2}$  and wind speed by *ca.*  $0.05 \text{ m}\cdot\text{s}^{-1}$ . It also showed that except for PBLH, AC dominated and dictated the spatial distribution and increase/decrease of the overall ACR effect on the downward shortwave radiation, cloud liquid water path, wind speed, and T2. AC and AR basically cancelled out each other leading to a small PBLH change due to the ACR interactions averaged over the entire domain. However, the regional difference of PBLH change was large and varied from a 50 m reduction to over a 100 m increase. SYN was generally a small contributor to the ACR effects on the studied meteorological parameters but played a relatively important role (*ca.* 25%) in the changes in wind speed.

### 3.3. Impact on Air Quality

Regional air quality is determined via a complex interaction among pollutant emissions, chemistry, advective and convective transport, as well as wet/dry deposition. The aforementioned changes in meteorological parameters due to the ACR effect would impose impacts on every aspect of an air quality system. They change biogenic, seasalt, and dust emissions. They alter photolysis rates and kinetics that lead to changes in chemical transformation [49]. They change transport and deposition processes. Altogether, they bring changes in surface ozone and PM<sub>2.5</sub> concentrations as illustrated in Figures 8 and 9, respectively.

AC dominated surface ozone changes due to the ACR interactions. Up to 2 ppbv changes, when averaged over three months, were found over land and ocean. Domain-wide, ACR interactions caused an approximately 0.4 ppbv reduction in the three-month average surface ozone concentration, or approximately 1.2% of the average from the experiment NoACR, in which AC accounted for *ca.* 67%. Spatially, changes in ozone over land generally followed the pattern of the T2 change—higher temperature typically favored ozone production with sufficient existence of nitrogen dioxide (NO<sub>x</sub>) and volatile organic compounds (VOC), two major ozone precursors, which was the case over most land areas. However, the southeast U.S. and eastern Texas experienced a relatively unchanged level or reduction in surface ozone even though a higher T2 was simulated there. Different mechanisms may be responsible. In the southeast U.S., biogenic VOC was abundant and ozone production was limited by the availability of NO<sub>x</sub> [43]. Higher T2 due to the ACR effect led to higher biogenic VOC emissions that would hinder ozone formation and accumulation in this NO<sub>x</sub>-limited region. In the eastern Texas, however, up to 1 ppbv ozone reduction was mainly explained by the 50–100 m increase in PBLH that tended to dilute surface pollutants. There was little change in surface ozone from the Rocky Mountains to the west coast areas of the U.S. due to the ACR interactions. Over the ocean, on the other hand, changes in ozone due to the ACR interactions followed the downward shortwave radiation change in an opposite way: higher downward shortwave radiation resulted in a lower surface ozone concentration. This was because higher downward shortwave radiation led to higher photochemical activity, which would destruct ozone where the ambient pollution level was low [50]. The finding that ozone over ocean decreased due to the ACR interactions was consistent with that reported by Forkel *et al.* [17].

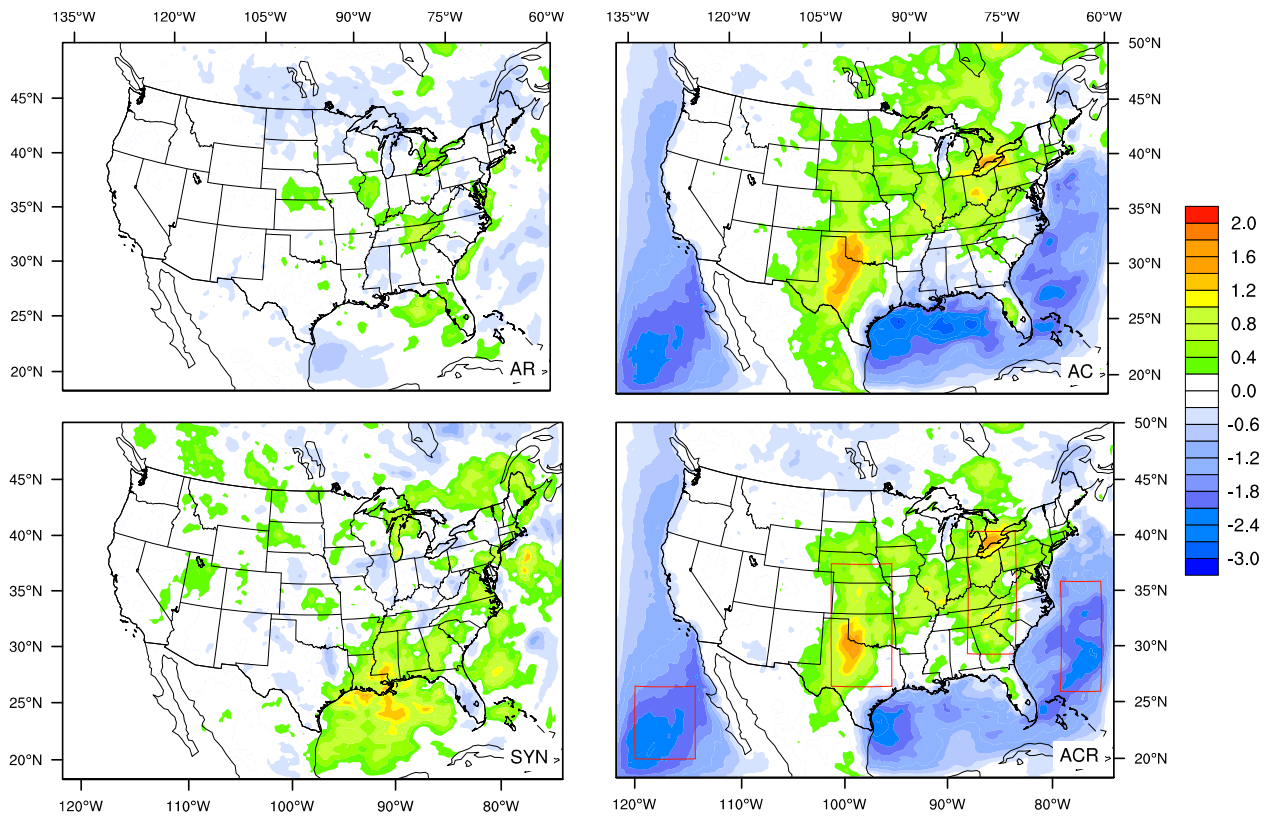


**Figure 8.** Spatial distribution of changes in the three-month average surface ozone concentration (ppbv) due to AR, AC, SYN, and ACR. Regions in red boxes are subject to temporal analysis.

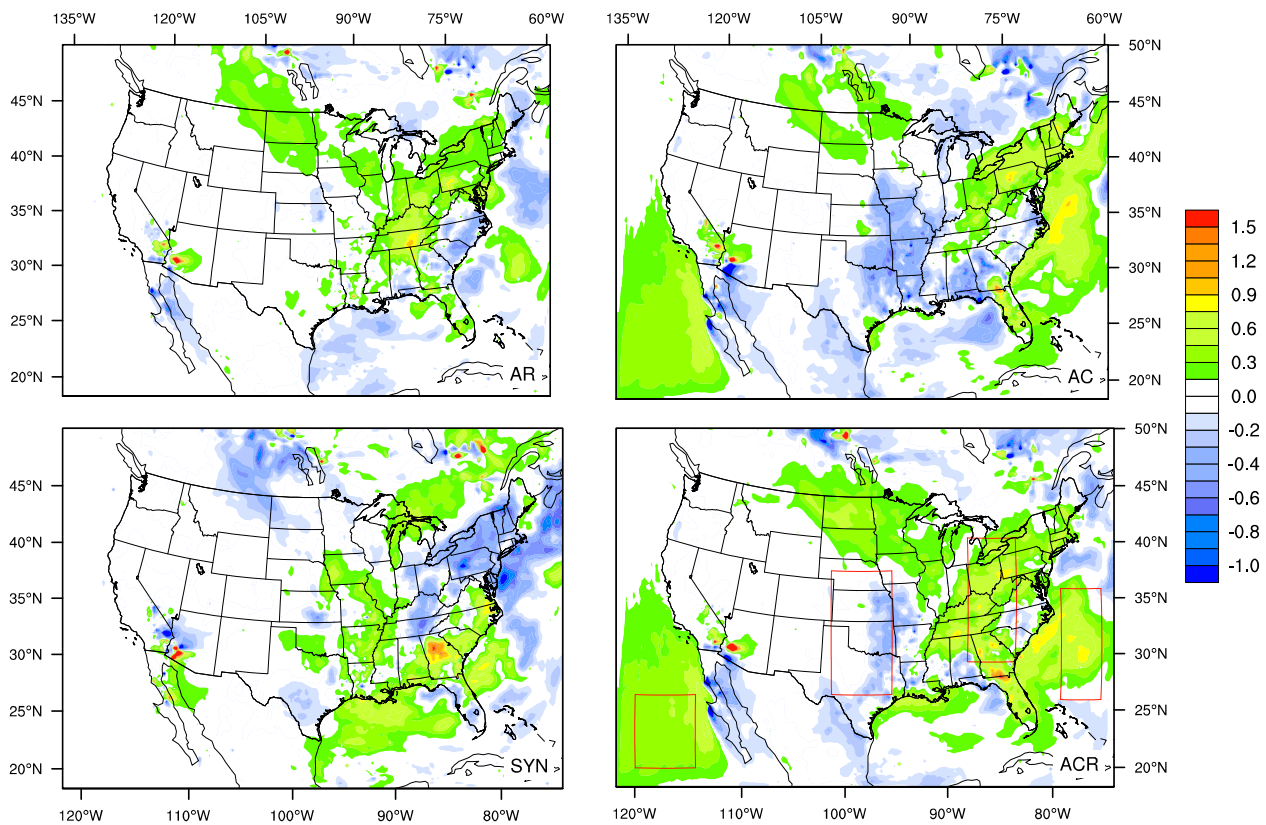


**Figure 9.** Same as Figure 8 except for surface PM<sub>2.5</sub> concentration ( $\mu\text{g}\cdot\text{m}^{-3}$ ).

Unlike the surface ozone change that was dominated by AC over both land and ocean, AC, AR, and SYN all contributed pronouncedly to surface PM<sub>2.5</sub> change due to the ACR interactions over land, while AC dominated over ocean. Domain-wide, a 0.1  $\mu\text{g}\cdot\text{m}^{-3}$  increase in the three-month average surface PM<sub>2.5</sub> concentration, which was *ca.* 1.3% of the domain average based on the experiment NoACR, was simulated with AC, AR, and SYN accounting for 52%, 27%, and 21%, respectively. A close examination revealed that surface PM<sub>2.5</sub> change mostly followed the changes in PBLH over land—a higher PBLH resulted in a lower PM<sub>2.5</sub> concentration, which also agrees with Forkel *et al.* [17]. Over the ocean, changes in both PBLH and wind speed played roles. Increased wind speed tended to introduce more sea salts into the atmosphere to lift the PM<sub>2.5</sub> concentration, especially over the Pacific adjacent to California and the Baja California Peninsula (figure not shown).

Although the domain-average three-month mean ACR effects were small, spatial and temporal variations of the impact of ACR interactions on surface ozone and PM<sub>2.5</sub> concentrations could be large, as illustrated in Figures 10 and 11, as well as in Table 4. In the selected “Pacific” region, the average daily surface ozone concentrations from the simulation NoACR decreased gradually from around 45 ppbv in early April to about 20 ppbv in late June. While AR and SYN on surface ozone oscillated along 0 and were within  $\pm 1$  ppbv, AC varied from 0 to  $-4.8$  ppbv over time. AC also dominated the ACR effect on surface PM<sub>2.5</sub> as time passed and generally increased the NoACR PM<sub>2.5</sub> by 0.1~1.5  $\mu\text{g}\cdot\text{m}^{-3}$ . However, SYN offset AC to bring the total ACR effect on surface PM<sub>2.5</sub> up to 1.0  $\mu\text{g}\cdot\text{m}^{-3}$ . On the regional average basis, the ACR interactions caused more than a 2.0 ppbv reduction in surface ozone and a 0.39  $\mu\text{g}\cdot\text{m}^{-3}$  increase in PM<sub>2.5</sub> concentration at the ground level.

The selected “Atlantic” region also experienced approximately a 1.8 ppbv reduction in surface ozone and a 0.38  $\mu\text{g}\cdot\text{m}^{-3}$  increase in PM<sub>2.5</sub> concentration, but its daily fluctuation was greater than that of the “Pacific” region. Different from the “Pacific” region, where AC almost always dominated ACR on surface ozone, AR and SYN in the “Atlantic” region were large on occasional days and SYN often counteracted AC, bringing a modest overall ACR effect over time. As mentioned earlier, over the selected “Pacific” and “Atlantic” regions, the aerosol-induced cloud liquid water path reduction led to more solar radiation reaching the surface (Table 4). This favored the ozone destruction in regions where emissions were limited [50]. Meanwhile, the decreased PBLH favored surface PM<sub>2.5</sub> accumulation.

In the selected “East US” region, the daily average surface ozone concentrations varied from around 35 to 60 ppbv, with the peak occurring in late May when the stagnant condition featuring high T<sub>2</sub> and downward shortwave radiation persisted. Coincidentally, the largest ACR of up to 17 ppbv and 4.5  $\mu\text{g}\cdot\text{m}^{-3}$  also occurred during that time period. A detailed meteorology analysis revealed that during that period, the ACR interaction strengthened the stagnant condition with the downward shortwave radiation and T<sub>2</sub> increasing by 90  $\text{W}\cdot\text{m}^{-2}$  and 4 K, respectively. Further analysis revealed that the ACR interaction also shifted wind direction to reduce the introduction of the moist Atlantic air into the eastern U.S., bringing down the cloud liquid water path by 70  $\text{g}\cdot\text{m}^{-2}$ . All these changes favored ozone and PM<sub>2.5</sub> production and accumulation. Though AC was still the main contributor to ACR, the importance of AR and SYN increased in this region. “East US” was also the only one in the selected regions that experienced both increased average surface ozone (by 0.62 ppbv) and PM<sub>2.5</sub> (by 0.39  $\mu\text{g}\cdot\text{m}^{-3}$ ).

The highlighted “Central US” area observed a domain-average 0.63 ppbv increase in surface ozone and a 0.07  $\mu\text{g}\cdot\text{m}^{-3}$  decrease in ground level PM2.5. The temporal variations were large, ranging from  $-1.5$  to 13.5 ppbv for ozone and from  $-1.0$  to 4.5  $\mu\text{g}\cdot\text{m}^{-3}$  for PM2.5 under the influence of ACR. The large temporal variations suggested that the ACR interactions depended strongly on meteorological conditions that changed from day-to-day, and could potentially bring large enough change that could affect the compliance of the national ambient air quality standard.

**Table 4.** Overall ACR effects on selected meteorological parameters and surface concentrations of ozone and PM2.5 for selected regions \*.

	SW ( $\text{W}\cdot\text{m}^{-2}$ )	QCW ( $\text{g}\cdot\text{m}^{-2}$ )	Wind@surface ( $\text{m}\cdot\text{s}^{-1}$ )	T (K)	PBLH (m)	Ozone (ppbv)	PM2.5 ( $\mu\text{g}\cdot\text{m}^{-3}$ )
Pacific	48.03	-87.03	0.03	0.11	-10.74	-2.03	0.39
Central_US	11.94	-40.66	0.05	0.50	37.24	0.63	-0.07
East_US	1.18	-12.89	0.10	0.34	14.25	0.62	0.39
Atlantic	7.40	-31.48	-0.03	0.07	-20.12	-1.81	0.38

\* SW = downward shortwave radiation; QCW = cloud liquid water path.

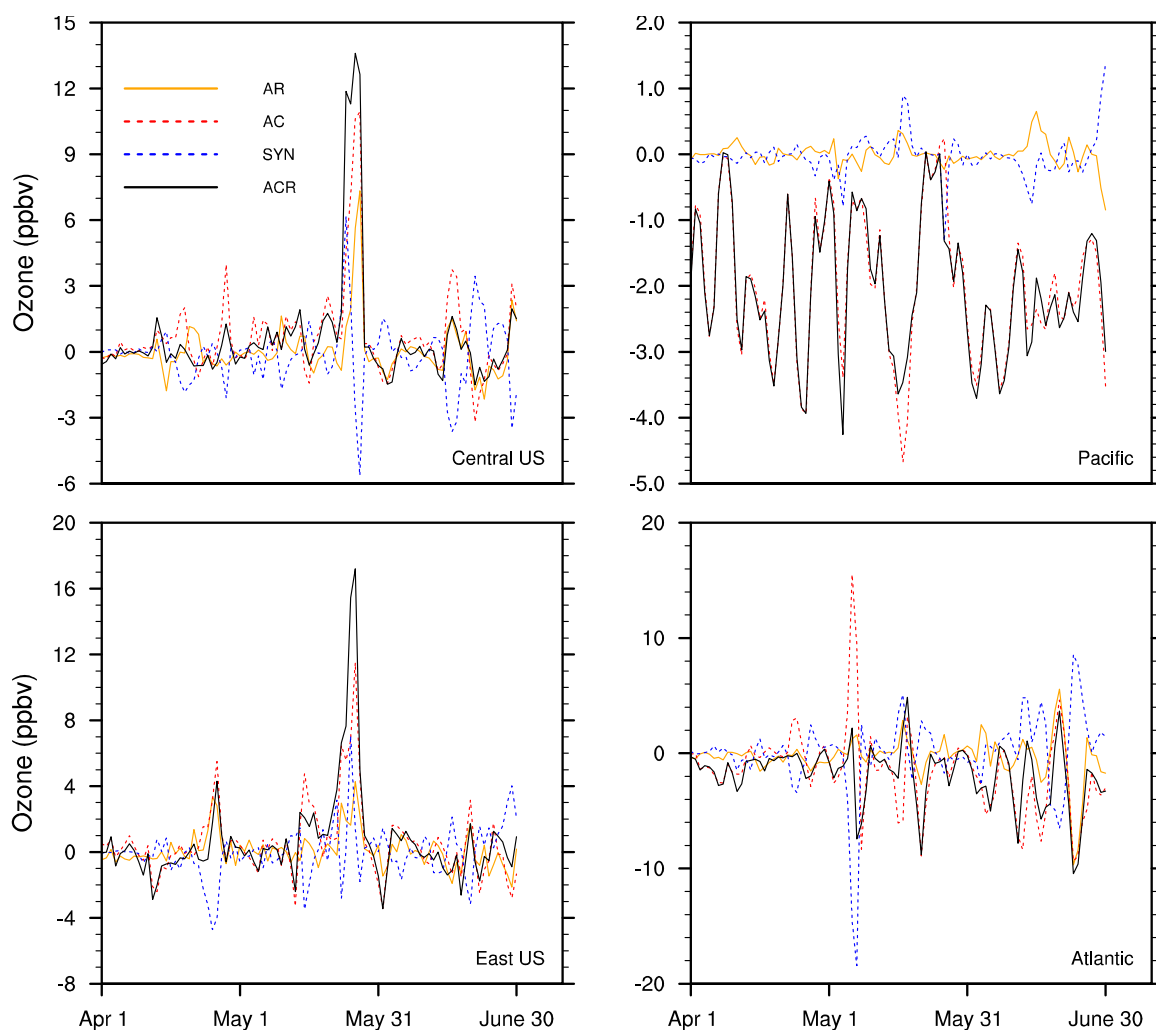


**Figure 10.** Temporal distributions of changes in surface ozone concentrations (ppbv) due to AC, AR, SYN, and ACR for the selected regions highlighted in red boxes of Figures 8 and 9.

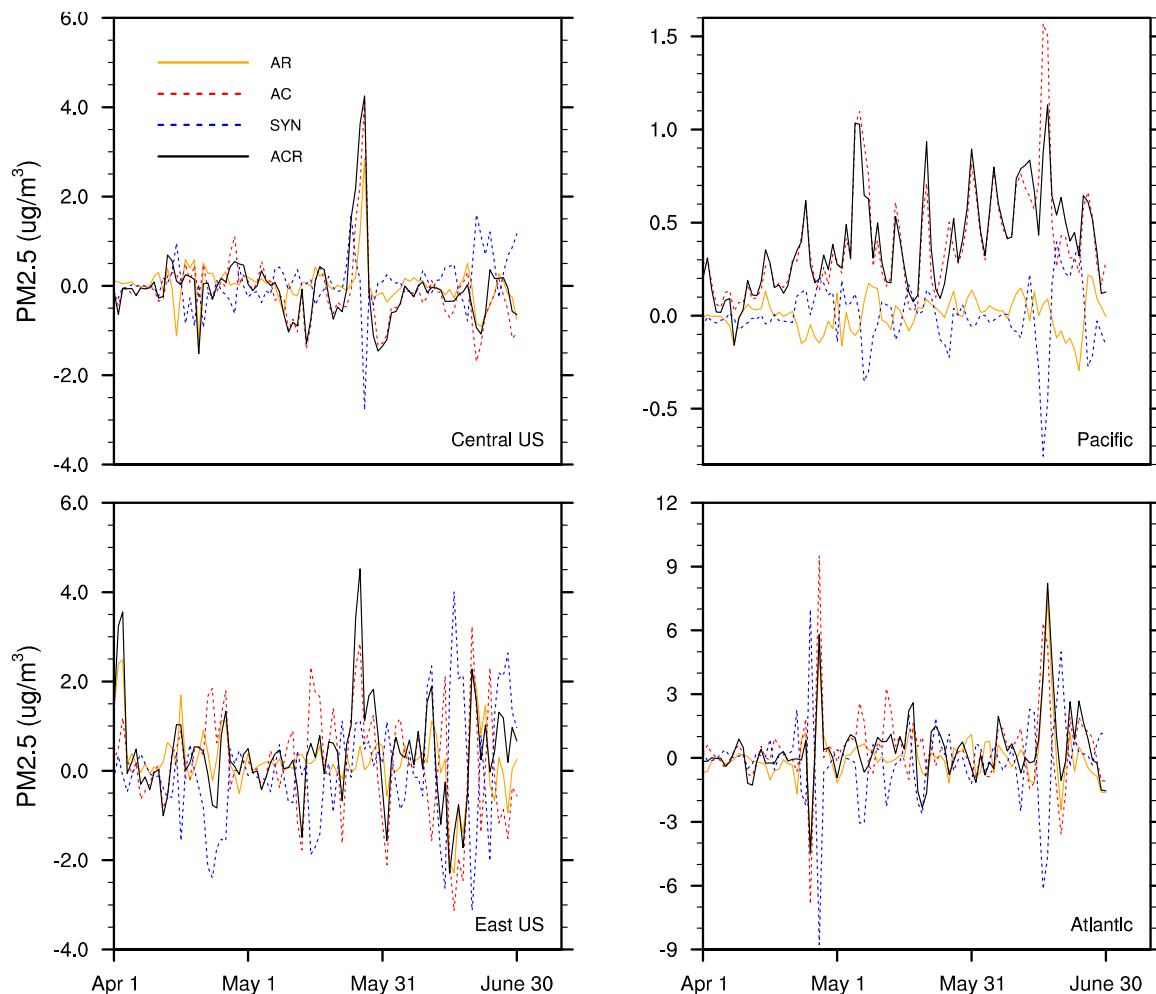


**Figure 11.** Same as Figure 10 except for surface PM<sub>2.5</sub> concentration ( $\mu\text{g}\cdot\text{m}^{-3}$ ).

#### 4. Summary and Conclusions

The NU-WRF model equipped with full ACR interactions was employed to investigate how such interactions can impact regional meteorology and the resultant air quality, focusing on surface ozone and PM<sub>2.5</sub>, over the continental U.S. To separate the impact from AC and AR, a factor separation technique was applied that also identified the synergistic impact (SYN) induced from AC and AR. Based on the case study that covered April through June of 2010, the following results were found:

1. The domain-average downward shortwave radiation reduced by  $4.2 \text{ W}\cdot\text{m}^{-2}$  due to AR. The aerosol effect, through directly absorbing and scattering solar radiation, can only explain part of the changes. The cloud change due to AR can explain the downward shortwave radiation changes in the eastern Texas and the mid-Atlantic Ocean for this case study.
2. In comparison with AR, AC had more influence on the atmospheric energy balance. It generally caused more precipitation ( $0.1 \text{ mm}\cdot\text{day}^{-1}$  averaged over the domain) and less cloud formation, which allowed a domain-average  $12.2 \text{ W}\cdot\text{m}^{-2}$  more downward shortwave radiation.
3. SYN, representing the nonlinear interaction between AC and AR, could either enhance or counteract them depending on location. SYN decreased the cloud formation and increased the downward shortwave radiation by  $0.2 \text{ W}\cdot\text{m}^{-2}$  averaged over the entire domain.

- Overall, AC dominated the effect of ACR interactions, especially for surface radiation energy and clouds, suggesting it plays a larger role in the weather system than AR. The domain-average overall ACR effect would reduce cloud coverage and wind speed while increasing downward shortwave radiation, surface temperature, and PBLH, as shown in Table 3. The spatial-temporal variations in the ACR effects were large.
- The ACR interaction-induced meteorology change would impose noticeable effects on surface ozone and PM<sub>2.5</sub>, especially over oceans and the eastern U.S. Domain-wide, ACR interactions caused an approximately 0.4 ppbv reduction and 0.1  $\mu\text{g}\cdot\text{m}^{-3}$  increase in three-month average surface ozone and PM<sub>2.5</sub> concentrations, respectively. However, the spatial-temporal variations were large and a more than 10 ppbv surface ozone and a 5  $\mu\text{g}\cdot\text{m}^{-3}$  PM<sub>2.5</sub> difference induced by the ACR interactions occurred frequently in the eastern U.S. and the Atlantic Ocean. The mechanism that led to surface PM<sub>2.5</sub> and ozone change varied from region to region, dependent upon the local chemical background (e.g., NO<sub>x</sub>- vs. VOC-sensitive regime), emissions, and meteorological conditions.

There were caveats to this study, though. The horizontal resolution was not fine enough to resolve clouds and aerosol-cloud interactions in the sub-grid convective cloud were not accounted for. Thus, the results may be biased. Future study with cloud-resolving resolution (less than 3 km) is warranted to examine the effect of ACR interactions on air quality over the U.S. In addition, the results shown here only represented one particular spring episode. Since it also depends on the prevailing meteorology [17], the effects of ACR interactions in other seasons need to be further investigated. Nevertheless, the finding that air quality changed pronouncedly in response to the ACR interactions may pose additional challenges in air quality management and compliance.

### Acknowledgments

The authors would like to thank the NASA Center for Climate Simulation (NCCS) for supercomputing support. This research was funded by NASA's Atmospheric Composition: Modeling and Analysis (ACMAP) program and the Modeling, Analysis, and Prediction (MAP) program.

### Author Contributions

Zhining Tao and Hongbin Yu made the experimental design and Zhining executed the numerical experiment. Zhining, Hongbin, and Mian Chin contributed to the result analysis.

### Conflicts of Interest

The authors declare no conflict of interest.

### References

- Charlson, R.J.; Schwartz, S.E.; Hales, J.M.; Cess, R.D.; Coakley, J.A., Jr.; Hansen, J.E.; Hofmann, D.J. Climate forcing by anthropogenic aerosols. *Science* **1992**, *255*, 423–430, doi:10.1126/science.255.5043.423.

2. Ackerman, A.S.; Toon, O.B.; Stevens, D.E.; Heymsfield, A.J.; Ramanathan, V.; Welton, E.J.; Reduction of tropical cloudiness by soot. *Science* **2000**, *288*, 1042–1047, doi:10.1126/science.288.5468.1042.
3. Twomey, S. The influence of pollution on the shortwave albedo of clouds. *J. Atmos. Sci.* **1977**, *34*, 1149–1152.
4. Yu, H.; Liu, S.C.; Dickinson, R.E. Radiative effects of aerosols on the evolution of the atmospheric boundary layer. *J. Geophys. Res.* **2002**, *107*, doi:10.1029/2001JD000754.
5. Zhang, Y.; Fu, R.; Yu, H.; Dickinson, R.E.; Juarez, R.N.; Chin, M.; Wang, H. A regional climate model study of how biomass burning aerosol impacts land-atmosphere interactions over the Amazon. *J. Geophys. Res.* **2008**, *113*, doi:10.1029/2007JD009601.
6. Barbaro, E.; Vilà-Guerau de Arellano, J.; Ouwensloot, H.G.; Schröter, J.S.; Donovan, D.P.; Krol, M.C. Aerosols in the convective boundary layer: Shortwave radiation effects on the coupled land-atmosphere system. *J. Geophys. Res. Atmos.* **2014**, *119*, 5845–5863, doi:10.1002/2013JD021237.
7. Zhang, Y.; Fu, R.; Yu, H.; Qian, Y.; Dickinson, R.E.; SilvaDias, M.A.F.; daSilvaDias, P.L.; Fernandes, K. Impact of biomass burning aerosol on the monsoon circulation transition over Amazonia. *Geophys. Res. Lett.* **2009**, *36*, doi:10.1029/2009GL037180.
8. Zhao, C.; Liu, X.; Leung, L.R. Impact of the Desert dust on the summer monsoon system over Southwestern North America. *Atmos. Chem. Phys.* **2012**, *12*, 3717–3731.
9. Ge, C.; Wang, J.; Reid, J.S. Mesoscale modeling of smoke transport over the Southeast Asian Maritime Continent: Coupling of smoke direct radiative effect below and above the low-level clouds. *Atmos. Chem. Phys.* **2014**, *14*, 159–174.
10. Grell, G.A.; Baklanov, A. Integrated modeling for forecasting weather and air quality: A call for fully coupled approaches. *Atmos. Environ.* **2011**, *45*, 6845–6851.
11. Grell, G.A.; Emeis, S.; Stockwell, W.R.; Schoenemeyer, T.; Forkel, R.; Michalakes, J.; Knoche, R.; Seidl, W. Application of a multiscale, coupled MM5/chemistry model to the complex terrain of the VOTALP valley campaign. *Atmos. Environ.* **2000**, *34*, 1435–1453.
12. Grell, G.A.; Peckham, S.E.; Schmitz, R.; McKeen, S.A.; Frost, G.; Skamarock, W.C.; Eder, B. Fully coupled “online” chemistry within the WRF model. *Atmos. Environ.* **2005**, *39*, 6957–6975.
13. Vogel, B.; Vogel, H.; Bäumer, D.; Bangert, M.; Lundgren, K.; Rinke, R.; Stanelle, T. The comprehensive model system COSMO-ART—Radiative impact of aerosol on the state of the atmosphere on the regional scale. *Atmos. Chem. Phys.* **2009**, *9*, 8661–8680, doi:10.5194/acp-9-8661-2009.
14. Baklanov, A.; Schlünzen, K.; Suppan, P.; Baldasano, J.; Brunner, D.; Aksoyoglu, S.; Carmichael, G.; Douros, J.; Flemming, J.; Forkel, R.; *et al.* Online coupled regional meteorology chemistry models in Europe: Current status and prospects. *Atmos. Chem. Phys.* **2014**, *14*, 317–398, doi:10.5194/acp-14-317-2014.
15. Jacobson, M.Z. Development and application of a new air pollution modeling system. Part III: Aerosol-phase simulation. *Atmos. Environ.* **1997**, *31*, 587–608.
16. Zhang, Y.; Wen, X.-Y.; Jang, C.J. Simulating chemistry-aerosol-cloud-radiation-climate feedbacks over the continental U.S. using the online-coupled Weather Research Forecasting Model with chemistry (WRF/Chem). *Atmos. Environ.* **2010**, *44*, 3568–3582.

17. Forkel, R.; Werhahn, J.; Hansen, A.B.; McKeen, S.; Peckham, S.; Grell, G.; Suppan, P. Effect of aerosol-radiation feedback on regional air quality—A case study with WRF/Chem. *Atmos. Environ.* **2012**, *53*, 202–211.
18. Boucher, O.; Randall, D.; Artaxo, P.; Bretherton, C.; Feingold, G.; Forster, P.; Kerminen, V.-M.; Kondo, Y.; Liao, H.; Lohmann, U.; *et al.* Clouds and Aerosols. In *Climate Change 2013: The Physical Science Basis. Contribution of Working Group I to the Fifth Assessment Report of the Intergovernmental Panel on Climate Change*; Stocker, T.F., Qin, D., Plattner, G.-K., Tignor, M., Allen, S.K., Boschung, J., Nauels, A., Xia, Y., Bex, V., Midgley, P.M., Eds.; Cambridge University Press: Cambridge, UK; New York, NY, USA, 2013; pp. 571–657.
19. Stein, U.; Alpert, P. Factor separation in numerical simulations. *J. Atmos. Sci.* **1993**, *50*, 2107–2115.
20. Michalakes, J.; Chen, S.; Dudhia, J.; Hart, L.; Klemp, J.; Middlecoff, J.; Skamarock, W. Development of a next generation regional weather research and forecast model. In Proceedings of the Ninth ECMWF Workshop on the Use of High Performance Computing in Meteorology, Reading, UK, 13–17 November 2000; pp. 269–276.
21. Santanello, J.A.; Peters-Lidard, C.D.; Kennedy, A.; Kumar, S.V. Diagnosing the nature of land-atmosphere coupling: A case study of dry/wet extremes in the U.S. Southern Great Plains. *J. Hydrometeorol.* **2013**, *14*, 3–24, doi:10.1175/JHM-D-12-023.1.
22. Tao, Z.; Santanello, J.A.; Chin, M.; Zhou, S.; Tan, Q.; Kemp, E.M.; Peters-Lidard, C.D. Effect of land cover on atmospheric processes and air quality over the continental United States—A NASA Unified WRF (NU-WRF) model study. *Atmos. Chem. Phys.* **2013**, *13*, 6207–6226, doi:10.5194/acp-13-6207-2013.
23. Peters-Lidard, C.D.; Kemp, E.M.; Matsui, T.; Santanello, J.A., Jr.; Kumar, S.V.; Jacob, J.P.; Clune, T.; Tao, W.-K.; Chin, M.; Hou, A.; *et al.* Integrated modeling of aerosol, cloud, precipitation and land processes at satellite-resolved scales. *Environ. Model. Softw.* **2015**, *67*, 149–159.
24. Chin, M.; Ginoux, P.; Kinne, S.; Torres, O.; Holben, B.N.; Duncan, B.N.; Martin, R.V.; Logan, J.A.; Higurashi, A.; Nakajima, T. Tropospheric aerosol optical thickness from the GOCART model and comparisons with satellite and Sun photometer measurements. *J. Atmos. Sci.* **2002**, *59*, 461–483.
25. Koehler, K.A.; Kreidenweis, S.M.; DeMott, P.J.; Prenni, A.J.; Carrico, C.M.; Ervens, B.; Feingold, G. Water activity and activation diameters from hygroscopicity data—Part II: Application to organic species. *Atmos. Chem. Phys.* **2006**, *6*, 795–809, doi:10.5194/acp-6-795-2006.
26. Andreae, M.O.; Rosenfeld, D. Aerosol–cloud–precipitation interactions. Part 1. The nature and sources of cloud-active aerosols. *Earth-Sci. Rev.* **2008**, *89*, 13–41.
27. DeMott, P.J.; Prenni, A.J.; Liu, X.; Kreidenweis, S.M.; Petters, M.D.; Twohy, C.H.; Richardson, M.S.; Eidhammer, T.; Rogers, D.C. Predicting global atmospheric ice nuclei distributions and their impacts on climate. *Proc. Natl. Acad. Sci. USA* **2010**, *107*, 11217–11222.
28. Shi, J.J.; Matsui, T.; Tao, W.-K.; Tan, Q.; Peters-Lidard, C.; Chin, M.; Pickering, K.; Guy, N.; Lang, S.; Kemp, E.M. Implementation of an aerosol-cloud microphysics-radiation coupling into the NASA Unified WRF: Simulation results for the 6–7 August 2006 AMMA Special Observing Period. *Q. J. R. Meteorol. Soc.* **2014**, doi:10.1002/qj.2286.

29. Tao, W.-K.; Shi, J.J.; Chen, S.S.; Lang, S.; Lin, P.-L.; Hong, S.-Y.; Peters-Lidard, C.; Hou, A. The impact of microphysical schemes on hurricane intensity and track. *Asia-Pac. J. Atmos. Sci.* **2011**, *47*, 1–16.
30. Chou, M.-D.; Suarez, M.J. *A Solar Radiation Parameterization (CLIRAD-SW) for Atmospheric Studies*; NASA Tech. Rep. NASA/TM-1999-10460; Washington, DC, USA, 1999; Volume 15, pp. 1–38.
31. Ek, M.B.; Mitchell, K.E.; Lin, Y.; Rogers, E.; Grunmann, P.; Koren, V.; Gayno, G.; Tarpley, J.D. Implementation of Noah land surface model advances in the National Centers for Environmental Prediction operational mesoscale Eta Model. *J. Geophys. Res.* **2003**, *108*, 8851, doi:10.1029/2002JD003296.
32. Hong, S.Y.; Noh, Y.; Dudhia, J. A new vertical diffusion package with an explicit treatment of entrainment processes. *Mon. Weather Rev.* **2006**, *134*, 2318–2341.
33. Grell, G.A.; Devenyi, D. A generalized approach to parameterizing convection combining ensemble and data assimilation techniques. *Geophys. Res. Lett.* **2002**, *29*, 1693, doi:10.1029/2002GL015311.
34. Lin, M.; Holloway, T.; Carmichael, G.R.; Fiore, A.M. Quantifying pollution inflow and outflow over East Asia in spring with regional and global models. *Atmos. Chem. Phys.* **2010**, *10*, 4221–4239, doi:10.5194/acp-10-4221-2010.
35. Stockwell, W.R.; Middleton, P.; Chang, J.S.; Tang, X. The Second Generation Regional Acid Deposition Model Chemical Mechanism for Regional Air Quality Modeling. *J. Geophys. Res.* **1990**, *95*, 16343–16367.
36. Gross, A.; Stockwell, W. R. Comparison of the EMEP, RADM2 and RACM Mechanisms. *J. Atmos. Chem.* **2003**, *44*, 151–170.
37. Emmons, L.K.; Walters, S.; Hess, P.G.; Lamarque, J.-F.; Pfister, G.G.; Fillmore, D.; Granier, C.; Guenther, A.; Kinnison, D.; Laepple, T.; *et al.* Description and evaluation of the Model for Ozone and Related chemical Tracers, version 4 (MOZART-4). *Geosci. Model Dev.* **2010**, *3*, 43–67.
38. Wiedinmyer, C.; Akagi, S.K.; Yokelson, R.J.; Emmons, L.K.; Al-Saadi, J.A.; Orlando, J.J.; Soja, A.J. The Fire INventory from NCAR (FINN): A high resolution global model to estimate the emissions from open burning. *Geosci. Model Dev.* **2011**, *4*, 625–641.
39. Guenther, A.; Karl, T.; Harley, P.; Wiedinmyer, C.; Palmer, P.I.; Geron, C. Estimates of global terrestrial isoprene emissions using MEGAN (Model of Emissions of Gases and Aerosols from Nature). *Atmos. Chem. Phys.* **2006**, *6*, 3181–3210.
40. Ginoux, P.; Chin, M.; Tegen, I.; Prospero, J.; Holben, B.; Dubovik, O.; Lin, S.-J. Sources and global distributions of dust aerosols simulated with the GOCART model. *J. Geophys. Res.* **2001**, *106*, 20255–20273.
41. Gong, S.L. A parameterization of sea-salt aerosol source function for sub- and super-micron particles. *Glob. Biogeochem. Cycles* **2003**, *17*, 1097, doi:10.1029/2003GB002079.
42. Thunis, P.; Cuvelier, C. Impact of biogenic emissions on ozone formation in the Mediterranean area—A BEMA modeling study. *Atmos. Environ.* **2000**, *34*, 467–481.
43. Tao, Z.; Larson, S.M.; Wuebbles, D.J.; Williams, A.; Caughey, M. A summer simulation of biogenic contributions to ground-level ozone over the continental United States. *J. Geophys. Res.* **2003**, *108*, 4404, doi:10.1029/2002JD002945.

44. Tao, Z.; Larson, S.; Williams, A.; Caughey, M.; Wuebbles, D.J. Sensitivity of regional ozone concentrations to temporal distribution of emissions. *Atmos. Environ.* **2004**, *38*, 6279–6285.
45. Xie, P.; Yatagai, A.; Chen, M.; Hayasaka, T.; Fukushima, Y.; Liu, C.; Yang, S. A gauge-based analysis of daily precipitation over East Asia. *J. Hydrometeorol.* **2007**, *8*, 607–626.
46. Chen, M.; Shi, W.; Xie, P.; Silva, V.B.S.; Kousky, V.E.; Higgins, R.W.; Janowiak, J.E. Assessing objective techniques for gauge-based analyses of global daily precipitation. *J. Geophys. Res.* **2008**, *113*, doi:10.1029/2007JD009132.
47. Tao, W.-K.; Li, X. Physical processes determining precipitation enhancement induced by CCN concentrations. *J. Geophys. Res.* **2015**, submitted.
48. Yang, Q.; Gustafson, W.I., Jr.; Fast, J.D.; Wang, H.; Easter, R.C.; Morrison, H.; Lee, Y.-N.; Chapman, E.G.; Spak, S.N.; Mena-Carrasco, M.A. Assessing regional scale predictions of aerosols, marine stratocumulus, and their interactions during VOCALS-Rex using WRF-Chem. *Atmos. Chem. Phys.* **2011**, *11*, 11951–11975, doi:10.5194/acp-11-11951-2011.
49. Seinfeld, J.H.; Pandis, S.N. *Atmospheric Chemistry and Physics—From Air Pollution to Climate Change*, 2nd ed.; John Wiley & Sons: New York, NY, USA, 2006; p. 1326.
50. Murazaki, K.; Hess, P. How does climate change contribute to surface ozone change over the United States? *J. Geophys. Res.* **2006**, *111*, doi:10.1029/2005JD005873.

© 2015 by the authors; licensee MDPI, Basel, Switzerland. This article is an open access article distributed under the terms and conditions of the Creative Commons Attribution license (<http://creativecommons.org/licenses/by/4.0/>).